L-shell ionization study of indium, tin, and rhenium by low-energy electron impact

Changhuan Tang,*[1,2] Zhengming Luo,[2] Zhu An,[2] Fuqing He,[2] Xiufeng Peng,[2] and Xianguan Long[2]
[1]*National Key Laboratory of Laser Fusion, Research Center of Laser Fusion, China Academy of Engineering Physics, P.O. Box 919-986, Mianyang, Sichuan 621900, People's Republic of China*
[2]*Key Laboratory for Radiation Physics and Technology of Education Ministry of China, Institute of Nuclear Science and Technology, Sichuan University, Chengdu 610064, People's Republic of China*
(Received 27 November 2001; published 18 April 2002)

The $L\alpha$, L_β, and $L\gamma$ x-ray production cross sections of In, Sn, and Re by electron impact were measured at energies from near threshold to tens of keV. Thin targets with thick substrates were used in the experiments. We compare the experimental results of Sn x-ray production cross sections with data determined by Baxter and Spicer [Aust. J. Phys. **36**, 287 (1983)] with a different method, and present some results. The measured x-ray production cross sections are also compared with the binary encounter approximation theory of Gryzinski [Phys. Rev. **138**, A336 (1965)] and the atomic-rearrangement theory of McGuire [Phys. Rev. A **16**, 73 (1977)]. It is found that the *L*-shell production cross sections do not exhibit a gradual increase with atomic number, a result observed by Park *et al.* [Phys. Rev. A **12**, 1358 (1975)] in a systematic study of *L*-shell x-ray production cross sections by MeV electron impact. For the present measured *L*-shell data of In and Sn, it seems that, so far, none of the available theories can adequately interpret the *L*-shell results at low energies.

DOI: 10.1103/PhysRevA.65.052707 PACS number(s): 34.80.Dp, 32.30.Rj

I. INTRODUCTION

The ionization of atoms by electron impact is a process of great importance in atomic and molecular physics. This has resulted in a much better understanding of both the theoretical and experimental aspects of electron-atom collisions. The data obtained can be used in such diverse fields as radiation physics, plasma physics, atmospheric physics, astrophysics, and electron microscopy. In many of these application areas, absolute cross sections for inner-shell ionization are required over a wide energy region [1–3], for example, in electron probe microanalysis (EPMA), Auger electron spectroscopy (AES), fusion research, and so on. These cross sections are also an important theoretical subject. A variety of theoretical treatments, beginning with that of Bethe [4], have been developed in an attempt to describe this process, either in classical or quantum mechanics.

During the past decade, the study of atomic inner-shell ionization by electron impact has been of growing interest both experimentally [5–14] and theoretically [6,15–17]. For example, Khare and Wadehra [15,17] employed the plane-wave Born approximation (PWBA) with exchange, Coulomb, and relativistic corrections and included the transverse interaction of virtual photons with atoms as well. Luo and Joy [16] performed an extensive series of calculations using first-order perturbation theory and Hartree-Slater wave functions for *K*, *L* (L_1 and L_{23}), and *M* (M_1, M_{23}, and M_{45}) shell ionization cross-sections for incident electron energies ranging from near threshold to 100 keV. Experimental research for atomic inner-shell ionization cross sections has been reported by Shevelko, Solomon, and Vukstich [5], Schneider *et al.* [6], Klovet, Morlet, and Salvat [18], and An *et al.*, Luo *et al.*, He *et al.*, Peng *et al.*, and Tang *et al.* [8–14]. Most of these data are for *K*-shell ionization, and the situation with *L* or higher shell is far from satisfactory. For *L*-shell ionization, the existing experimental data are concentrated on high-energy electron-induced x-ray production cross sections or ionization cross sections [26–30], and some of these data are merely given as relative cross-section ratios. The increasing complexities of the multiple decay channels following *L*- and higher-shell ionization are largely responsible for the more limited data for the relevant inner-shell ionization cross sections as well as for the associated fluorescence yields and the Auger and Coster-Kronig transition probabilities. These complexities are also responsible for the generally poorer accuracy of the measured *L*- and higher-shell cross sections compared to *K*-shell data. Inspection of the currently available experimental data [20–23] reveals that they are still scarce for many elements and, when they are available one usually finds significant discrepancies between data from different authors [21], which are often much larger than the stated experimental uncertainties. More detailed reviews of the present status for inner-shell ionization are given in [18,19].

We generally measured atomic inner-shell x-ray production cross sections. Through a set of atomic parameters, such as the x-ray emission rate, fluorescence yields and Coster-Kronig transition probabilities (for *L*- and higher shells), the x-ray production cross sections can be converted to the corresponding ionization cross sections and vice versa. Two techniques can be used to measure *L*-shell x-ray production cross sections in both solid and gaseous targets. The decay products of *L*-shell ionization, either characteristic x-rays or Auger electrons, can be detected. The cross sections for the yields of x-rays or Auger electrons are of particular value since they can be applied directly in EPMA and AES.

In recent years, Luo *et al.*, have made major progress in measurements of *K*-shell ionization cross sections by low-energy electron impact [8–13]. In this paper, we extend the method to measurements of absolute *L*-shell x-ray produc-

*Author to whom correspondence should be addressed. Email address: C.H.Tang@263.net

TABLE I. Parameters for the calculation of In, Sn, and Re *L*-shell x-ray production cross sections [38].

Elements	Z	A	E_{L1} (keV)	E_{L2} (keV)	E_{L3} (keV)	ρd (μ g/cm^2)
In	49	114.82	4.238	3.938	3.730	9.4
Sn	50	118.69	4.465	4.156	3.929	9.4
Re	75	186.20	12.527	11.957	10.535	34.5

tion cross sections $\sigma^x_{L\alpha}$, $\sigma^x_{L_\beta}$, and $\sigma^x_{L\gamma}$, of indium, tin, and rhenium. This paper aims at checking the existing data and providing data for practical applications. The experimental data, for energies from near threshold to 40 keV for Re and for energies from near threshold to 25 keV for In and Sn, are reported. Comparisons are made of the experimental results with previous measurements and theoretical results. We also find a different trend of the dependence of the *L*-shell x-ray production cross sections on atomic number, and give a possible explanation.

II. EXPERIMENT

A detailed description of the present experimental setup has been given elsewhere [9,11], and here only a brief description is presented. The experimental setup is identical to one we used earlier [11]. The monoenergetic electron beam from near threshold to 40 keV was provided by an electron gun and adjusted in accordance with the x-ray counting rate; the energy of the incident electron beam was determined by the end point of the obtained bremsstrahlung spectrum. With this method, the incident electron energy could be measured within an uncertainty of 0.1 keV. The electron beam was well collimated and then hit the target, which was placed at 45° with respect to the direction of the incident beam. A horizontal Si(Li) detector was kept inside the vacuum chamber to reduce energy loss from air and was about 10 cm from the center of the target. The detector full width at half maximum was 170 eV for ^{55}Mn $K\alpha$ x rays. The detector efficiency was calibrated with a set of standard radioactive sources, i.e., ^{241}Am, ^{137}Cs, ^{55}Fe, and ^{54}Mn, provided by the China Institute of Standards and Technology. The uncertainty of the calibrated efficiency was believed to be less than 5%. All charges of the incident electron beam were collected by a

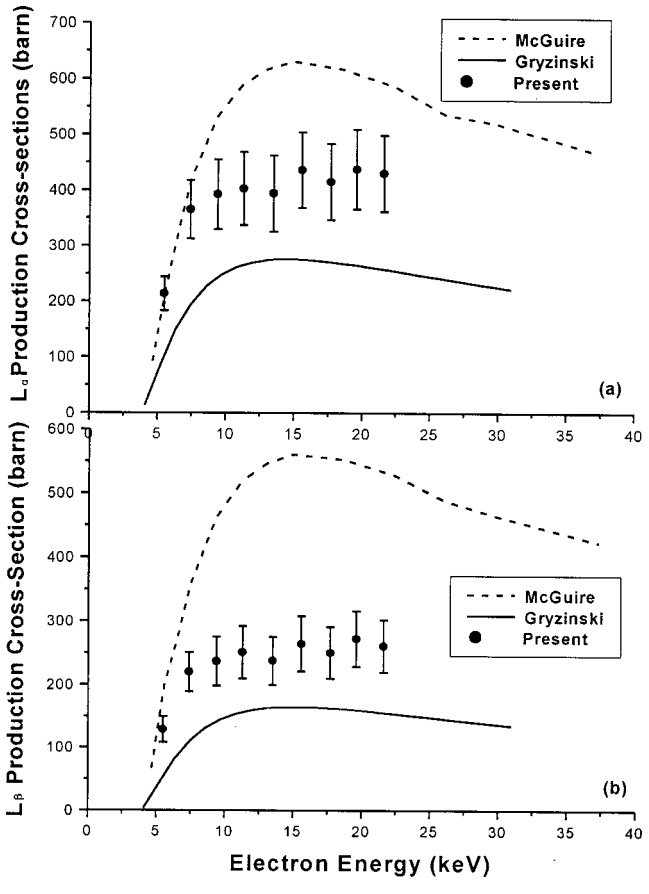

FIG. 1. In *L*-shell x-ray production cross sections $\sigma^x_{L\alpha}$ (a) and $\sigma^x_{L_\beta}$ (b) as a function of electron energy. The solid circles represent the present results. The solid line represents predictions of Gryzinski's theory [31]. Results calculated from McGuire's theory are shown by a dashed line [32].

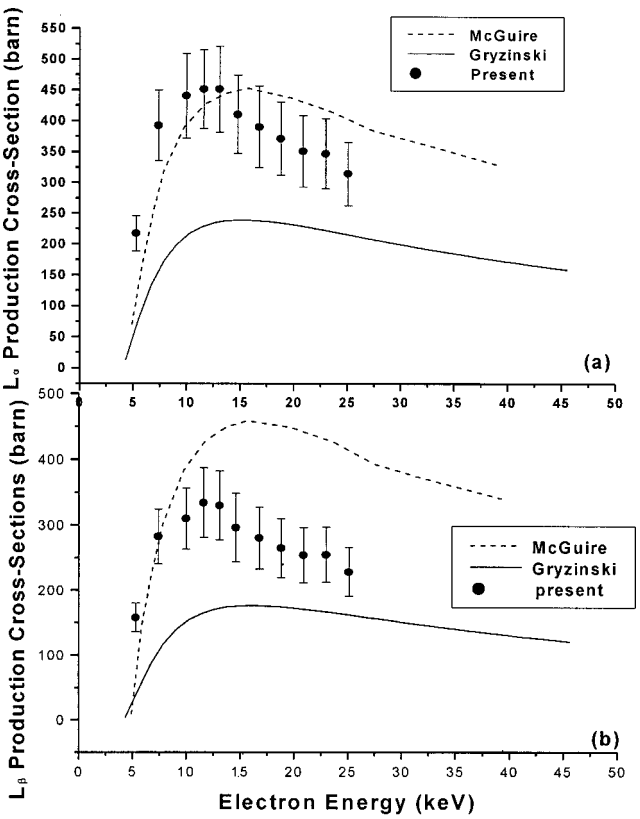

FIG. 2. Sn *L*-shell x-ray production cross sections $\sigma^x_{L\alpha}$ (a) and $\sigma^x_{L_\beta}$ (b) as a function of electron energy. The symbols are the same as those in Fig. 1.

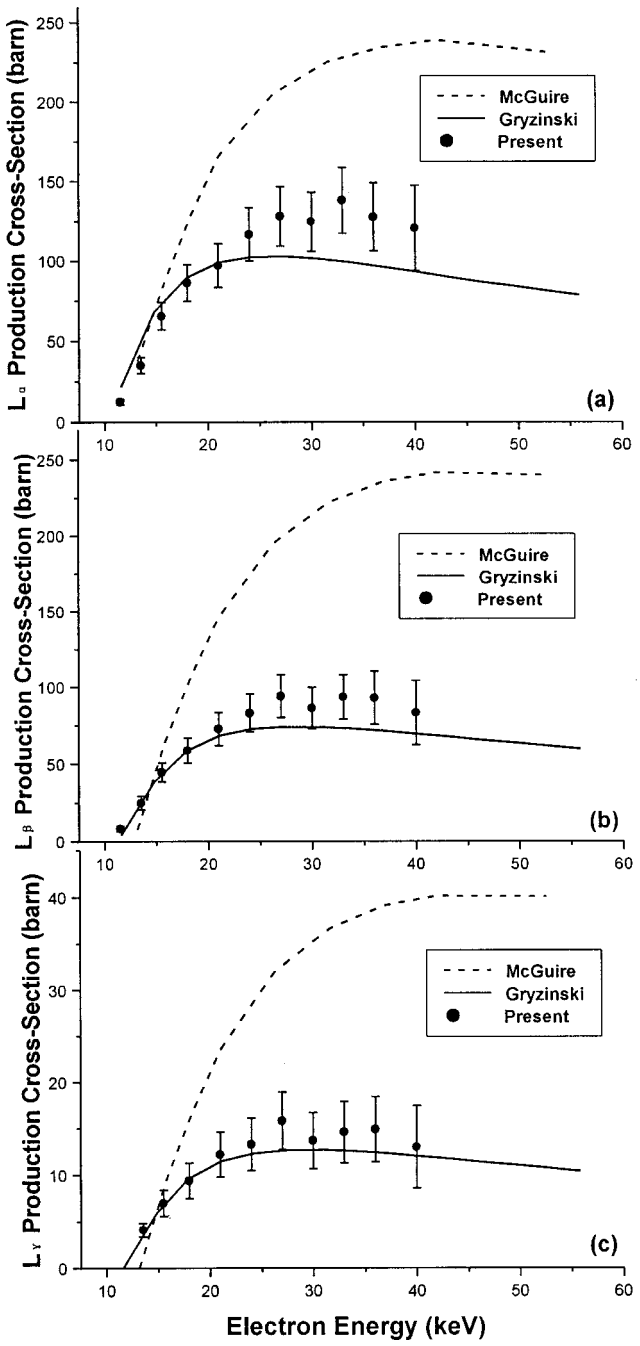

FIG. 3. Re *L*-shell x-ray production cross sections $\sigma^x_{L\alpha}$ (a), $\sigma^x_{L_\beta}$ (b), and $\sigma^x_{L\gamma}$ (c) as a function of electron energy. The symbols are the same as those in Fig. 1.

deep Faraday cup and were led to a digital current integrator. The current integrator was calibrated by a standard current before measurement and its uncertainty was found to be less than 0.3% [22].

The targets used in our experiments were prepared by evaporating elements directly onto an aluminum substrate. The film mass thicknesses were determined by weighing with a balance having a precision of 10^{-6} g. The target thicknesses are thin enough to make the energy loss of incident electrons less than 0.5% of the incident electron energy,

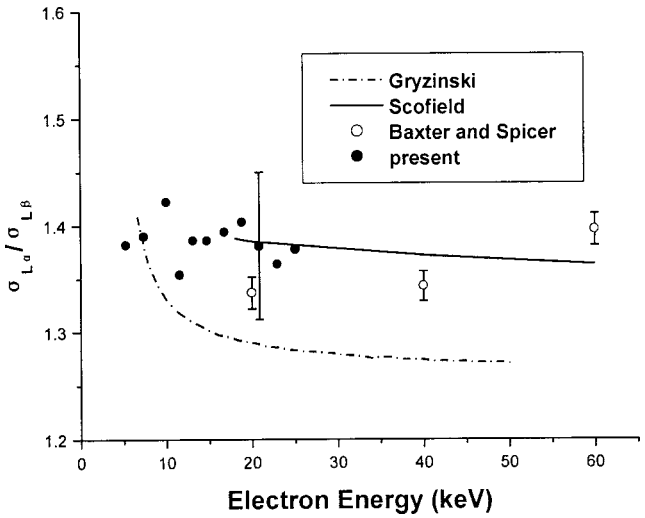

FIG. 4. Ratios of measured x-ray production cross section ratios $\sigma^x_{L\alpha}/\sigma^x_{L_\beta}$ for Sn (full circles) compared with the data of Baxter and Spicer [25] (open circles) as well as with theoretical calculations based on the RBA by Scofield [37] (solid line) and the BEA by Gryzinski [31] (dot-dashed line), respectively.

and are listed in Table I; the thickness uncertainty (one standard deviation) should be less than 10% [22].

III. RESULTS AND ANALYSIS

To determine the *L*-shell x-ray production cross sections σ^x_i $(i=L\alpha,L_\beta,L\gamma)$, we measured the number of characteristic x-rays counts N^x_i $(i=L\alpha,L_\beta,L\gamma)$ emitted from the target bombarded with N_e electrons of energy E_i. For a target of thickness d (in centimeters) and with its surface at an angle θ related to the incident beam direction, the *L*-shell x-ray production cross section can be expressed as

$$\sigma^x_i=\frac{4\pi N^x_i\cos\theta}{N_e dn\,\eta\Omega}\quad (i=L\alpha,L_\beta,L\gamma), \tag{1}$$

where n (in atoms/cm^3) and $\eta\Omega/4\pi$ are the atomic density and the total detection efficiency for characteristic x rays, respectively.

Due to the existence of a thick substrate, reflected electrons, whose energy exceeds the ionization threshold of the target atoms, can induce additional inner-shell ionizations that result in a systematic overestimation of the cross sections; corrections should be made for this effect. We have calculated the fraction of ionization events caused by electrons reflected from the aluminum substrate. The final expression for *L*-shell x-ray production cross sections can be written as

$$\sigma^x_i(E)=\frac{4\pi N^x_i\cos\theta}{N_e dn\,\eta\Omega}-\cos\theta\int_{E_i}^{E}\Phi_{\rm ref}(E')\sigma^x_i(E')dE' \tag{2}$$

where the subscript i indicates $L\alpha$, $L\beta$, $L\gamma$ and the second term indicates the fraction of ionization events caused by electrons reflected from the aluminum substrate. $\Phi_{\rm ref}$ the reflected energy spectrum, is calculated by using the so-called

TABLE II. Measured In, Sn, and Re L-shell x-ray production cross sections $\sigma^x_{L\alpha}$, $\sigma^x_{L_\beta}$, and $\sigma^x_{L\gamma}$, by electron impact. (E_i refers to incident electron energy; the numbers in parentheses refer to the total estimated one-standard-deviation uncertainty.)

In			Sn			Re			
E_i (keV)	$\sigma^x_{L\alpha}$ (barn)	$\sigma^x_{L_\beta}$ (barn)	E_i (keV)	$\sigma^x_{L\alpha}$ (barn)	$\sigma^x_{L_\beta}$ (barn)	E_i (keV)	$\sigma^x_{L\alpha}$ (barn)	$\sigma^x_{L_\beta}$ (barn)	$\sigma^x_{L\gamma}$ (barn)
5.5	213.4 (±30.2)	128.6 (±20.7)	5.3	217.0 (±28.8)	157.7 (±21.9)	11.5	12.5 (±1.8)	8.3 (±1.6)	0
7.4	365.0 (±52.3)	219.8 (±31.1)	7.4	392.3 (±57.2)	282.3 (±42.0)	13.5	35.1 (±4.9)	24.8 (±4.4)	4.1 (±0.7)
9.4	392.2 (±62.6)	236.7 (±38.4)	10.0	440.5 (±68.7)	309.8 (±46.7)	15.5	65.5 (±8.5)	44.5 (±6.3)	7.0 (±1.4)
11.3	402.6 (±65.8)	250.7 (±41.3)	11.6	451.2 (±63.4)	333.9 (±53.0)	18.0	86.2 (±11.4)	58.7 (±8.2)	9.4 (±1.9)
13.5	393.7 (±68.9)	237.5 (±37.8)	13.1	451.1 (±69.5)	329.8 (±52.5)	21.0	97.0 (±13.6)	72.7 (±10.7)	12.2 (±2.4)
15.6	436.3 (±68.3)	264.2 (±43.4)	14.6	410.2 (±63.3)	296.0 (±52.6)	24.0	116.7 (±16.7)	83.0 (±12.3)	13.3 (±2.8)
17.7	415.0 (±68.6)	250.2 (±40.7)	16.8	390.1 (±66.2)	279.9 (±47.2)	27.0	127.9 (±18.6)	94.0 (±14.0)	15.8 (±3.1)
19.6	437.5 (±71.8)	272.5 (±43.6)	18.8	371.1 (±59.4)	264.6 (±45.3)	30.0	124.6 (±18.6)	86.2 (±13.5)	13.7 (±3.0)
21.6	430.2 (±68.9)	260.8 (±41.4)	20.9	350.7 (±57.7)	253.9 (±42.2)	33.0	138.0 (±20.7)	93.4 (±14.6)	14.6 (±3.3)
			23.0	346.7 (±56.9)	254.3 (±42.4)	36.0	127.6 (±21.4)	92.9 (±17.3)	14.9 (±3.5)
			25.1	314.1 (±51.7)	228.0 (±37.8)	40.0	120.6 (±26.8)	83.3 (±21.0)	13.0 (±4.4)

bipartition model of electron transport [24]. After performing iterations with Eq. (2), the actual L-shell x-ray production cross sections can be obtained. The details have been given elsewhere [9].

Sn was selected since Baxter and Spicer [25] have published experimental data in part of the energy region of our measurements. Nevertheless, they reported only the relative x-ray production cross-section ratios $\sigma^x_{L\alpha}/\sigma^x_{L_\beta}$, $\sigma^x_{L\alpha}/\sigma^x_{L\gamma}$, and $\sigma^x_{L\alpha}/\sigma^x_{L_1}$. In our paper, we present absolute cross sections and ratios of cross sections for comparison with the existing data. The absolute L-shell x-ray production cross sections $\sigma^x_{L\alpha}$, $\sigma^x_{L_\beta}$, and $\sigma^x_{L\gamma}$ of In, Sn, and Re are plotted in Figs. 1–3, and the $\sigma^x_{L\alpha}/\sigma^x_{L_\beta}$ ratio is plotted in Fig. 4. Unfortunately, $L\gamma$ data for In and Sn could not be analyzed since the $L\gamma$ peak was too weak to be distinguished from the background. All of the present experimental results are listed in Table II. Errors mainly arise from counting statistics for the net peak counts (1–5 %), spectral fitting (<5%), detector efficiency (5%), target thickness (10%), inhomogeneity of the targets (3%), and correction for the influence of reflected electron (2%) [9]. Therefore, the total uncertainty (one standard deviation) is estimated to be less than 15%.

In Figs. 1–3, the measured L-shell x-ray production cross sections $\sigma^x_{L\alpha}$ and $\sigma^x_{L_\beta}$ for In and Sn as well as $\sigma^x_{L\alpha}$, $\sigma^x_{L_\beta}$, and $\sigma^x_{L\gamma}$ for Re are compared with two different theoretical calculations: the so-called binary encounter approximation (BEA) theory of Gryzinski [31] and the atomic rearrangement theory of McGuire [32]. For comparison with the experimental data, the L-shell ionization cross sections (σ_{L_1}, σ_{L_2}, and σ_{L_3}) obtained from theoretical calculations must be converted into x-ray production cross sections ($\sigma^x_{L\alpha}$, $\sigma^x_{L_\beta}$, and $\sigma^x_{L\gamma}$). The relation between L-shell ionization cross section and x-ray production cross section can be found in Ref. [29]. Conversion is quite straightforward but involves a set of atomic parameters, which presently have quite high-experimental errors (5–20 %) [33]. A number of literature sources are presently available. The most common sources are: Krause [33], Chen, Crasemann, and Mark [34], and Puri *et al.* [35] for fluorescent and Coster-Kronig yields and Scofield's tabulations of x-ray emission rates [36]. In this paper, the fluorescence yields and Coster-Kronig yields given by Krause and the x-ray emission rates from Scofield are used in order to compare with the results of Baxter and Spicer [25] on a consistent basis who used the same parameters to convert theoretical ionization cross sections to x-ray production cross sections. The x-ray emission rate, the fluorescence and Coster-Kronig yields used in the conversion calculation for the x-ray production cross sections are listed in Tables III and IV, respectively. In the conversion calculation, we have omitted the negligible contributions of L-shell vacancies created in filling K-shell vacancies by L-shell electrons.

It can be seen from Figs. 1–3 that the present experimental results do not follow trends expected from theory. The cross sections for In and Sn generally lie between the predicted values of McGuire and Gryzinski, while the cross sections of Re are consistent with Gryzinski's formula. The latter results are in agreement with other experiments. Although Gryzinski theory was deduced from a classical binary model,

TABLE III. X-ray emission rates (Γ) for In, Sn, and Re [36].

Elements	Γ_1	Γ_2	Γ_3	$\Gamma_{3\alpha}$	$\Gamma_{3\beta}$	$\Gamma_{2\beta}$	$\Gamma_{2\gamma}$	$\Gamma_{1\beta}$	$\Gamma_{1\gamma}$
In	0.0954	0.1593	0.1515	0.1311	0.01 548	0.1387	0.01 645	0.07 933	0.01 515
Sn	0.1066	0.1786	0.1696	0.1456	0.01 846	0.1545	0.01 967	0.08 804	0.01 765
Re	0.861	1.497	1.328	1.0644	0.21 166	1.215	0.24 721	0.6531	0.18 697

TABLE IV. Fluorescence yields (ω_i) and Coster-Kronig transition probabilities (f_{ij}) for tin [33].

Elements	Constants	ω_1	ω_2	ω_3	f_{12}	f_{13}	f_{23}
In	Values	0.020	0.061	0.060	0.10	0.59	0.157
	Uncertainties(%)	30–20	25–10	20–10	20	10	20
Sn	Values	0.037	0.065	0.064	0.17	0.27	0.157
	Uncertainties(%)	20–15	10	10–5	20	15	20
Re	Values	0.144	0.283	0.268	0.16	0.33	0.130
	Uncertainties(%)	15	5	5–3	20	10–5	15

it gives good agreement with experimental *L*-shell x-ray production cross sections for high-*Z* atoms in some energy regions [26,27,29]. For Sn, the shape of the energy dependence of our measured x-ray production cross sections is similar to that of Gryzinski, namely, the maximum cross section appears at or near $U=3$ (where U is the reduced energy defined as the ratio of the incident electron energy to the inner-shell ionization energy). However, the Gryzinski values are only about half of the experimental results. The values given by McGuire's theory are closer to the experimental data, although the peak in his curve appears near $U=4$. For In, however, neither of the two theories is in good agreement with the measured cross sections.

Since the errors in the x-ray production cross sections come mainly from the determination of target thickness and detector efficiency, the relative line intensities can be determined with higher accuracy. In Fig. 4, the measured $\sigma^x_{L\alpha}/\sigma^x_{L_\beta}$ intensity ratios for Sn are plotted and compared with the results of Baxter and Spicer [25] as well as with the theoretical data of Gryzinski [31] and Scofield [37]. Baxter and Spicer measured the ratios $\sigma^x_{L\alpha}/\sigma^x_{L_\beta}$ in the energy range from 20 to 100 keV. However, we measured these ratios from near threshold to 25 keV. It can be seen from Fig. 4 that our ratios are in good agreement with Baxter's results in the energy region of overlap (within our 5% experimental error at 20.9 keV). Using the relativistic form of the first-order Born approximation (RBA), Scofield [37] calculated ionization cross sections down to only 50 keV, similar to the range of the Baxter and Spicer results. An extrapolation based upon Scofield's polynomial fit was performed to enable comparisons with our data near 20 keV. We can see that the extrapolation of Scofield's theory is in reasonable agreement with our results for Sn. For the near-threshold data, there is a major discrepancy in the different trends of the $\sigma^x_{L\alpha}/\sigma^x_{L_\beta}$ ratios with incident electron energy between the experimental data and the predictions of the classical binary encounter approximation (BEA) model of Gryzinski.

Park, Smith, and Scholz [26] performed a systematic study of *L*-shell x-ray production and *L*-subshell ionization by MeV electrons. Cross sections were presented for 14 elements from Ba ($Z=56$) to Bi ($Z=83$) for electron energies of 1.04, 1.39, and 1.76 MeV. They found that the measured *L*-shell x-ray production cross sections exhibited a gradual increase with atomic number at all energies. In Fig. 5, we plot $\sigma^x_{L\alpha}$ (a) and $\sigma^x_{L_\beta}$ (b) for In, Sn, and Re together. Recently, absolute $L\alpha$, L_β, and $L\gamma$ x-ray production cross sections for W were reported by Peng *et al.* [14]. Values of $\sigma^x_{L\alpha}$ and $\sigma^x_{L_\beta}$ for W are also shown in Figs. 5(a) and 5(b), respectively. From Fig. 5, we can see the dependence of *L*-shell x-ray production cross section on atomic number. We find that the data for In and Sn intersect, and that the cross sections for these elements are larger than those of W and Re for the same energy. The dependence of x-ray production cross section on atomic number is different from that found by Park, Smith, and Scholz. It therefore appears that the cross section of electron-atom collisions must be different for the high- and low-energy regions. For high-energy electrons, cal-

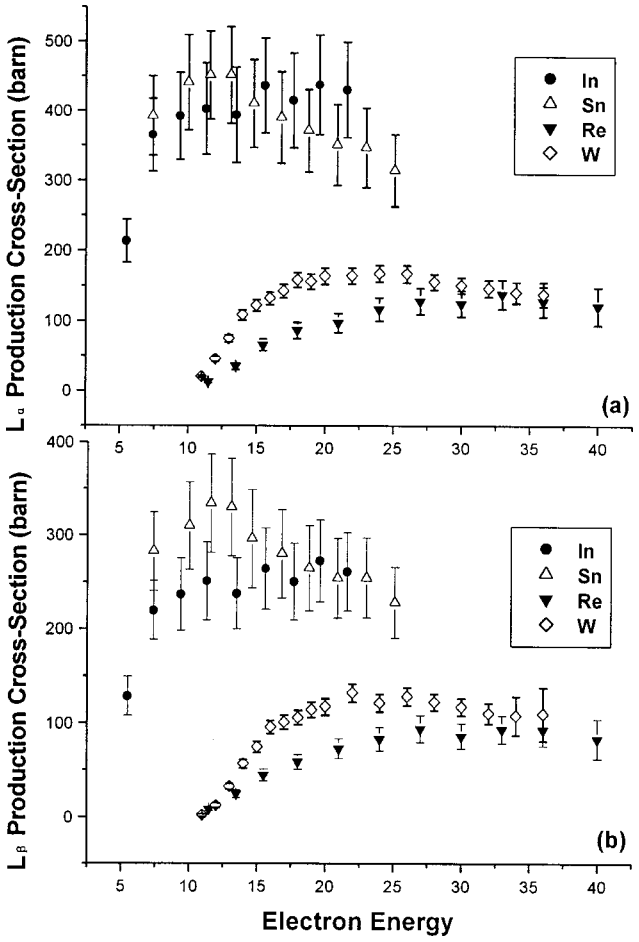

FIG. 5. Measured $\sigma^x_{L\alpha}$ (a) and $\sigma^x_{L_\beta}$ (b) of In, Sn, W [14], and Re are compared to one other.

culations of ionization cross sections within the plane-wave first Born approximation (PWBA) generally provide reliable results [29]. Further investigation is needed for describing the cross sections of electrons at near-threshold energies for which the Bethe equation [4] is thought to be invalid.

In conclusion, we have reported experimental absolute *L*-shell x-ray production cross sections for In, Sn, and Re. The Re *L*-shell x-ray production cross sections are in good agreement with the predictions of Gryzinski's theory. We find a different dependence of x-ray production cross section on atomic number than expected from the Gryzinski's theory. It seems that, so far, none of the available theories can adequately interpret the In and Sn *L*-shell results at low energies. Further investigation is needed, both experimentally and theoretically, for a better understanding of inner-shell ionization processes.

ACKNOWLEDGMENTS

This work was supported by the National Natural Science Foundation of China under Grant No. 19874045 and by the Key Project of the Education Ministry of China.

[1] C. J. Powell, Rev. Mod. Phys. **48**, 33 (1976).
[2] C. J. Powell, *Electron Impact Ionization*, edited by T. D. Mark and G. H. Dunn (Springer-Verlag, New York, 1985), Chap. 6.
[3] C. J. Powell, in *Microbeam Analysis*, edited by J. R. Michael and P. Ingram (San Francisco Press, San Francisco, 1990), p. 13.
[4] H. Bethe, Ann. Phys. (Leipzig) **5**, 325 (1930).
[5] V. P. Shevelko, A. M. Solomon, and V. S. Vukstich, Phys. Scr. **43**, 158 (1991).
[6] H. Schneider, I. Tobehn, E. F. Tobehn, and R. Hippler, Phys. Rev. Lett. **71**, 2707 (1993).
[7] R. Shanker and R. Hippler, Z. Phys. D: At., Mol. Clusters **42**, 161 (1997).
[8] Z. An, T. H. Li, L. M. Wang, and Z. M. Luo, Phys. Rev. A **54**, 3067 (1996).
[9] Z. M. Luo, Z. An, F. Q. He, T. H. Li, X. G. Long, and X. F. Peng, J. Phys. B **29**, 4001 (1996).
[10] Z. M. Luo, Z. An, T. H. Li, L. M. Wang, Q. Zhu, and X. Y. Xia, J. Phys. B **30**, 2681 (1997).
[11] F. Q. He, X. G. Long, X. F. Peng, Z. M. Luo, and Z. An, Nucl. Instrum. Methods Phys. Res. B **114**, 213 (1996); **129**, 445 (1997).
[12] X. F. Peng, F. Q. He, X. G. Long, Z. M. Luo, and Z. An, Phys. Rev. A **58**, 2034 (1998).
[13] C. H. Tang, Z. M. Luo, Z. An, and T. H. Li, Chin. Phys. Lett. **16**, 505 (1999).
[14] X. F. Peng, F. Q. He, X. G. Long, Z. An, and Z. M. Luo, Chin. Phys. Lett. **18**, 39 (2001).
[15] S. P. Khare and J. M. Wadehra, Can. J. Phys. **74**, 376 (1996).
[16] S. Luo, Ph.D. thesis, University of Tennessee, Knoxville, (1994); S. Luo and D. C. Joy, in *Microbeam Analysis*, edited by D. G. Howitt (San Francisco Press, San Francisco, 1991), p. 67.
[17] S. P. Khare, V. Saksena, and J. M. Wadehra, Phys. Rev. A **48**, 1209 (1993).
[18] X. Klovet, C. Merlet, and F. Salvat, J. Phys. B **33**, 3761 (2000).
[19] C. J. Powell (private communication).
[20] X. Long, M. Liu, F. Ho, and X. Peng, At. Data Nucl. Data Tables **45**, 353 (1990).
[21] D. C. Joy, Scanning **17**, 270 (1995).
[22] C. H. Tang, Ph.D. thesis, Sichuan University, Chengdu, People's Republic of China, (2000).
[23] M. T. Liu, Z. An, C. H. Tang, Z. M. Luo, X. F. Peng, and X. G. Long, At. Data Nucl. Data Tables **76**, 213 (2000).
[24] Z. M. Luo, Phys. Rev. B **32**, 812 (1985); **32**, 824 (1985).
[25] G. W. Baxter and B. M. Spicer, Aust. J. Phys. **36**, 287 (1983).
[26] Y. K. Park, Mary T. Smith, and W. Scholz, Phys. Rev. A **12**, 1358 (1975).
[27] B. Schlenk, D. Berenyi, S. Ricz, A. Valek, and G. Hock, J. Phys. B **10**, 1303 (1977).
[28] H. Genz, D. H. H. Hoffmann, W. Low, and A. Richter, Phys. Lett. **73A**, 313 (1979).
[29] J. Palinkas and B. Schlenk, Z. Phys. A **297**, 29 (1980).
[30] P. N. Johnston, B. M. Spicer, and R. Helstroom, J. Phys. B **14**, 1077 (1981).
[31] M. Gryzinski, Phys. Rev. **138**, A336 (1965).
[32] E. J. McGuire, Phys. Rev. A **16**, 73 (1977).
[33] M. O. Krause, J. Phys. Chem. Ref. Data **8**, 307 (1979).
[34] M. H. Chen, B. Crasemann, and H. Mark, Phys. Rev. A **24**, 177 (1981).
[35] S. Puri, D. Mehta, B. Chand, Nirmal Singh, and P. N. Trehan, X-Ray Spectrom. **22**, 358 (1993).
[36] J. H. Scofield, At. Data Nucl. Data Tables **14**, 121 (1974).
[37] J. H. Scofield, Phys. Rev. A **18**, 963 (1978).
[38] Y. Z. Liu, *Decay Scheme of the Usual Radioisotopes* (Atomic Energy Press, Beijing, 1982) (in Chinese).